THREE-BODY HALO NUCLEI IN THE HYPERSPHERICAL HARMONICS METHOD

by

PRAVEN ARJUNA NAIDOO

Submitted in accordance with the requirements for the degree of

MASTER OF SCIENCE

in the subject of

PHYSICS

at the

UNIVERSITY OF SOUTH AFRICA

SUPERVISOR: PROF. G. J. RAMPHO

NOVEMBER 2020

Declaration

Student :Praven Arjuna Naidoo

Student No. :55388051

I declare that **"THREE-BODY HALO NUCLEI IN THE HYPERSPHERICAL HARMONICS METHOD"** is my own work and that all the sources that I have used or quoted have been indicated and acknowledged by means of complete references.

SIGNATURE

08/01/2021

DATE

Acknowledgement

- I would like to thank my supervisor Prof G.J Rampho for his patience and expert guidance throughout this research.
- I would like thank my family for their support and encouragement during my research.

Summary

Substantial progress has been made in the studies of loosely-bound nuclei, however there are many issues about the properties of these nuclei that have not been resolved yet. For example nuclear decay, nuclear reactions and nuclear structure remain open questions. Despite the large amount of information on proton and neutron halo systems, there are structural similarities and differences in these nuclei that are yet to be fully understood. The purpose of this study is to theoretically investigate structural properties of the light halo nuclei ^{8}B, ^{6}He, ^{6}Li,^{6}Be,^{9}Be and ^{9}B. In this study, these nuclei are treated as three-body systems interacting through standard potentials. The Faddeev equations for these potentials are solved using the hyperspherical harmonic methods. The ground-state energy, root-mean square radius and wavefunctions were calculated and the results obtained were compared with theoretical and experimental results reported in literature.

Key words

Three-body systems, halo nuclei, Faddeev equations, hyperspherical harmonic method, two-body potentials.

Contents

List of Figures

List of Tables

Chapter 1

Introduction

There are various types of nuclei such as unstable and stable nuclei. Some unstable nuclei have an excess of protons or neutrons. That is, nuclei that lie below or above the valley of stability and are radioactive. Studies into unstable nuclei have led to discoveries of new nuclear structures such as 'nuclei skin', when there is excess neutrons distributed on the surface of a nucleus and 'halo nuclei', when neutrons are found far beyond the nuclear core [1]. Stable nuclei are not radioactive, and are found on the band of stability and have low energy states. Light nuclei generally have a mass number of less than 50 and are stable when the amount of protons is equal to the amount of neutrons [2]. Heavy nuclei require more neutrons in the nucleus to be more stable to overcome the increase in electrostatic repulsion.

A halo nucleus is defined as a nucleus that has a core, containing nucleons, where the last one or two valence nucleons are very weakly bound [3]. In a halo nucleus, more than 50% of probability density of the valence nucleons is found outside the range of the core potential which accounts for their larger size and low separation energy. Halo nuclei have a very short lifetime and generally have only one bound state. The valence nucleons have a low orbital angularmomentum because higher angularmomentum would lead to a rise in the centrifugal barrier. Two neutron halo nuclei, known as Borromean systems, have no two-body subsystems bound states. They have narrow momentum distributions compared to stable nuclei and are found on the edges of the neutron and proton dripline. The Coulomb force for the proton halo nuclei means that the valence proton is located closer to the core than the neutron halo nuclei, hence this makes the proton rich nuclei rarer and more difficult to identify.

The discovery of halo nuclei has sparked interest in the understanding of such nuclei. Hence, there are many studies of weakly bound nuclear systems that lie far from the band of stability [4]. Studies of halo nuclei further contribute to the understanding of interactions in the motion of nucleus with low density, asymmetric nuclei, weakly bound three body systems, nucleosynthesis [5], two proton decay [6], Borromean systems [7] and to better examine astrophysical data [8]. Despite the large amount of information on proton and neutron halo systems, there are structural similarities and differences in these nuclei that are yet to be fully understood. The purpose of this study is to theoretically investigate structural properties of the light halo nuclei ^{8}B, ^{6}He, ^{6}Li,^{6}Be,^{9}Be and ^{9}B.

The Faddeev equations for a system three particles are a set of three coupled equations that describe three possible interactions and exchanges in a three-particle system [9]. The Faddeev equations are used to study three-body scattering with short-range interactions and require the potential between interacting pairs of particles as inputs. Faddeev equations can be solved by various methods. One method is done without angularmomentum decomposition [10]. This method applies to the Faddeev equations in momentum space. Also, this method is useful because limited partial waves provides limited qualitative insight as in three bound nucleon state calculations which require many different isospin, spin and orbital angularmomentum combinations. The Faddeev equations have been used [11] in scattering processes and bound state computations. The Faddeev equations are able to treat interactions [12] that depend on the spin, isospin and angularmomentum. The coordinate space Faddeev equations can be used for long range interaction like that of the Coulomb potential which involves many partial waves.

The Faddeev equations have been applied in low energy multiple scattering [13] of three nucleon systems using an approximation scheme that preserves the unitarity of bound and scattering states of the system. To define the low energy of nucleon to nucleon interactions, the approximation utilizes non-local separable potentials. Properties of three-nucleon systems are studied with nucleon-nucleon tensor and short-range interactions which are represented by phenomenological potentials. This method has also been applied to the neutron-deuteron scattering problem and the triton binding energy problem which are treated exactly. The three-body Faddeev equations have been used in the n-d scattering above the breakup threshold problem [14]. In this method, the Faddeev equations are solved in configuration space and is based on a finite basis set expansion of the Faddeev components. The Faddeev

equations have also been applied to solve the boundary problem which describes the scattering process and allows to obtain scattering parameters from the asymptotic representation of the wavefunction.

The Faddeev equations are applied to solve for bound state energies [15], by using the separable t-matrix approximations which are solvable using the inner structure quantum numbers of the particles and including spin. They have been calculated for ^{9}Be, ^{6}Li, ^{12}C nuclei and the results calculated agree well with the experimental values. The t-matrix approximations together with the Faddeev equations have been utilized to calculate the scattering amplitudes for electron capture from neutral hydrogen by fast protons [16]. The influence on the three-body capture amplitude originates from the on-energy shell two-body t-matrix. It was observes that the capture amplitude was indistinguishable from Drisko's second Born-approximation computation, aside from an energy-dependent phase factor which eventually approaches unity with adequately high incident energy.

The Faddeev equations are utilized [17] to determine the aggregate and differential cross segments for the dissociative connection of an electron to H_2, HD, and D_2, atoms (e + AB $\rightarrow$ A^- + B). The adiabatic estimation (at electron energies over the edge for the separation of the particle to the free atoms A + B) and the estimation of distinguishable potentials (at electron energies beneath this limit) are estimations to tackle the Faddeev equations. Great understanding is accomplished between theoretical estimations and experimental information on dissociative connection.

The three potentials in the Schrödinger equation are replaced by permutation operators, which are universal and easy to implement in three-body problems [18]. This can transform the Faddeev amplitudes from their natural coordinate system into the other coordinate systems. The Faddeev equations are well suited when the interacting particle has no interaction with the spectator particle. In configuration space, the singularities can be explained with the correct asymptotic behaviour of the wavefunction. When there are identical particles, the equation can be replaced by one equation since the equations become independent.

In the hyperspherical harmonic expansion method [19], each Faddeev amplitude is expanded in a series of complete bases functions that depend on a set of collective variables involving

the hyperradius and five angular variables. The hyperspherical harmonic angular functions are eigenfunctions of the square of hyperangularmomentum operator. The study of ^{11}Li and ^{6}He three particles systems with two neutron halos use the Faddeev equations along with the hyperspherical harmonic method.

There are various numerical methods to solve the three-body Schrödinger equation [11], with the separated centre of mass motion. These include the finite element, finite difference and variational methods. The techniques created in this field are founded on three-body equations that give an accurate depiction of the of the quantum mechanical three-body frameworks [20]. The variational methods generate very accurate solutions with an increasing number of variational parameters. However, direct solutions of the three-body Schrödinger equation are preferred. The disadvantage of variational methods is that the variational wavefunction is selected arbitrarily.

The hyperspherical harmonic method, [21], provides a good clear picture of the system in configuration space wavefunction. The method is a useful tool for determining the solution of the Schrödinger equations, the coordinate system is stated in terms of six coordinates after the centre of mass is separated. These coordinates comprise of one hyperradial variable and five hyperangular variables [11]. The wavefunction in these coordinates is expressed as a sum of products of the hyperradial and hyperangular functions. The three-body centre of mass Schrödinger equation uses the hyperspherical harmonic method by reducing it to a set of coupled equations in a single variable [22].

There are several advantages for using the hyperspherical harmonic method [22]. The properties of convergence of the expansions are known and all transformations of the three particles can be described by the rotation group. With the exception for truncation of the expansion basis, the hyperspherical harmonic method involves no approximation [23]. By examining the rate of convergence while progressively expanding the expansion basis, one can choose in principle the precision of the binding energy. In practice, there is a slow convergence of the series of the hyperspherical harmonic method [11].

One disadvantage [11] of the hyperspherical harmonic method is that there is large degeneracy in the hyperspherical basis, this is because of the rotation of the system and the three degrees of freedom are not completely separated from the internal degrees of freedom. Having a large

hyperangularmomentum quantum numbers increases the expansion basis which increases the number of coupled equations and hence increases the difficulty in the numerical solutions [23].

The hyperspherical harmonic method is widely used in bound states in atomic, nuclear and particle physics [21]. An application of the hyperspherical harmonic method has been used to examine the properties of the ${}^{6}_{\Lambda\Lambda}$He hyper nucleus treated as a three-body systems [23]. This method was also used to study the spectra of a variety of atomic and molecular systems [24]. This method was used to solve the Schrödinger equation for a variety of quantum mechanical systems [25].

This dissertation is organized as follows. In Chapter 2, the Jacobi and hyperspherical coordinate systems are explained and the notations are outlined. The quantum mechanical equations used are also given. In Chapter 3, the results and analysis are compared with theoretical and experimental studies in the literature. In Chapter 4 the significance of the results obtained is discussed.

Chapter 2

Hyperspherical Formalism

There are various numerical methods to solve the three-body Schrödinger equation [11], with the separated centre of mass motion. These include the finite element, finite difference and variational methods. The techniques created in this field are founded on three-body equations that give an accurate depiction of the of the quantum mechanical three-body frameworks [20]. The variational methods [11], generate very accurate solutions with an increasing number of variational parameters. However, direct solutions of the three-body Schrödinger equation are preferred. The disadvantage of variational methods is that the variational wavefunction is selected arbitrarily.

2.1 Jacobi Coordinates

Consider a system of three particles each with position vector $\vec{r_i}$, $\vec{r_j}$ and $\vec{r_k}$. The relative motion of the particles is described by Jacobi coordinates shown in Figure 2.1 below [26]

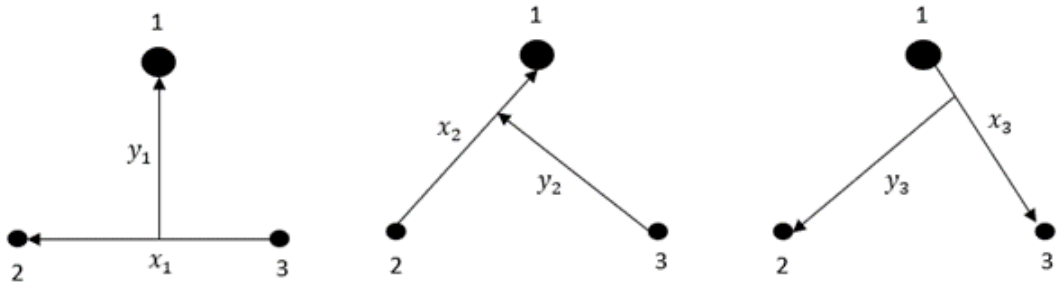

Figure 2.1: Three sets of Jacobi vectors for a system of three particles.

The Jacobi vectors $(\vec{x_i}, \vec{y_i})$ for the system can be defined as

$$\begin{aligned} \vec{x_i} &= \sqrt{A_{jk}}\vec{r_{jk}} \\ \vec{y_i} &= \sqrt{A_{(jk)i}}\vec{r_{(jk)i}}. \end{aligned} \tag{2.1}$$

The separation vector between interacting particles j and k, denoted by $\vec{r_{jk}}$, and the separation vector between the centre-of-mass of the interacting pair and the third particle i, denoted by $\vec{r_{(jk)i}}$ are defined by

$$\begin{aligned} \vec{r_{jk}} &= \vec{r_j} - \vec{r_k} \\ \vec{r_{(jk)i}} &= \vec{r_i} - \frac{A_j\vec{r_j} + A_k\vec{r_k}}{A_j + A_k}. \end{aligned} \tag{2.2}$$

The corresponding reduced mass is defined as

$$\begin{aligned} A_{jk} &= \frac{A_j\, A_k}{A_j + A_k} \\ A_{(jk)i} &= \frac{A_i(A_j + A_k)}{A_i + A_j + A_k}, \end{aligned} \tag{2.3}$$

where $i, j, k \in (1, 2, 3)$ with $A_i = \dfrac{m_i}{m}$, m is a unit mass and m_i the mass of particle i.

2.2 Hyperspherical coordinates

The Jacobian coordinates are then transformed into hyperspherical coordinates defined as [21]

$$\begin{aligned} x_i &= \rho\cos\phi_i \\ y_i &= \rho\sin\phi_i \end{aligned} \tag{2.4}$$

where $\rho = \sqrt{x_i^2 + y_i^2} = \sum_{i=1}^{3} A_i r_i^2$ is the hyperradial coordinate which is invariant under translation, rotation and permutation of the particles. The hyperangle $\phi_i = \arctan\left(\dfrac{x_i}{y_i}\right)$ together with the spherical polar angles $(\theta_{x_i}, \phi_{x_i})$ and $(\theta_{y_i}, \phi_{y_i})$ of $\vec{x_i}$ and $\vec{y_i}$ make up the five angular coordinates and are denoted by

$$\Omega \to \{\phi_i, \theta_{x_i}, \phi_{x_i}, \theta_{y_i}, \phi_{y_i}\} \tag{2.5}$$

which are dependent on the Jacobi partition.

2.3 Hyperspherical Harmonic Expansion Method

In the six hyperspherical variables (ρ, Ω_i), the kinetic energy operator has the form [21]

$$-\frac{\hbar^2}{2\mu}\left(\frac{\partial^2}{\partial x^2} + \frac{\partial^2}{\partial y^2}\right) = -\frac{\hbar^2}{2\mu}\left\{\frac{1}{\rho^5}\frac{\partial}{\partial\rho}\left(\rho^5\frac{\partial}{\partial\rho}\right) - \frac{\hat{\mathcal{K}}^2(\Omega_i)}{\rho^2}\right\} \tag{2.6}$$

where the interaction potential $\hat{\mathcal{K}^2}(\Omega_i)$ is the square of hyperangularmomentum operator specified as

$$\hat{\mathcal{K}^2}(\Omega_i) = -\frac{\partial^2}{\partial\phi_i^2} - 4\cot\phi_i + \frac{\partial}{\partial\phi_i} + \frac{1}{\cos^2\phi_i}\hat{l^2}(\hat{x_i}) + \frac{1}{\sin^2\phi_i}\hat{l^2}(\hat{y_i}) \tag{2.7}$$

where $\hat{l^2}(\hat{y_i})$ and $\hat{l^2}(\hat{y_i})$ are the squares of the ordinary orbital angular momenta associated with $\vec{x_i}$ and $\vec{y_i}$ vectors. The operator $\hat{\mathcal{K}^2}(\Omega_i)$ satisfies the eigenvalue equation below

$$\hat{\mathcal{K}^2}(\Omega_i)\,\mathcal{Y}_{K\alpha_i}(\Omega_i) = K(K+4)\mathcal{Y}_{K\alpha_i}(\Omega_i) \tag{2.8}$$

where $\mathcal{Y}_{K\alpha_i}(\Omega_i)$ are the normalized eigenfunctions, called hyperspherical harmonics, defined by

$$\mathcal{Y}_{K\alpha_i}(\Omega_i) = N_K^{l_{x_i}l_{y_i}}(\cos\phi_i)^{l_{x_i}}(\cos\phi_i)^{l_{y_i}}P_{n_i}^{l_{y_i}+\frac{1}{2},l_{x_i}+\frac{1}{2}}(\cos 2\phi_i) \tag{2.9}$$

where $P_n^{\alpha,\beta}$ are Jacobi polynomial with normalisation $N_K^{l_{x_i}l_{y_i}}$ and K_i is the hyperangularmomentum defined by

$$K_i = l_{x_i} + l_{y_i} + 2n_i\ (n_i = 0, 1, 2, ...). \tag{2.10}$$

In 6-dimensional space on a unit hypersphere, the hyperspherical harmonics form a complete set of orthogonal functions. The transformation which connects the three corresponding Jacobi coordinates sets are defined by [21]

$$\begin{aligned}\vec{x}_k &= -cos\varphi_{ki}\vec{x}_i + sin\varphi_{ki}\vec{y}_i \\ \vec{y}_k &= -sin\varphi_{ki}\vec{x}_i - cos\varphi_{ki}\vec{y}_i\end{aligned} \tag{2.11}$$

where $\varphi_{ki} = tan^{-1}\left\{(-1)^P\sqrt{\frac{AA_j}{A_iA_k}}\right\}$, and P being even if (i,j,k) is an even permutation and odd if (i,j,k) is an odd permutation. Under kinetic rotation, the quantum numbers $K,\ L,\ M$ remain the same. The parity of the hyperspherical harmonics are also conserved [27].

The hyperspherical harmonics, $\mathcal{Y}_{K\alpha_i}(\Omega_i)$ can be expanded in terms of $\mathcal{Y}_{K\alpha_j}(\Omega_j)$ through a unitary transformation defined by

$$\mathcal{Y}_{K\alpha_i}(\Omega_i) = \sum_{\alpha_j}\langle\alpha_j|\alpha_i\rangle_{KL}\mathcal{Y}_{K\alpha_j}(\Omega_j) \tag{2.12}$$

where $K,\ L,\ M$ are conserved and there is rotational degeneracy with respect to quantum number M for spin independent forces. As a result

$$\langle\alpha_j|\alpha_i\rangle_{KL} = \left\langle l_{x_j}l_{y_j}\middle|l_{x_i}l_{y_i}\right\rangle_{KL} \tag{2.13}$$

Eq. (2.12) can be written as

$$\mathcal{Y}_{K\alpha_i}(\Omega_i) = \sum_{l_{x_j}l_{y_j}}\left\langle l_{x_j}l_{y_j}\middle|l_{x_i}l_{y_i}\right\rangle_{KL}\mathcal{Y}_{K\alpha_j}(\Omega_j) \tag{2.14}$$

where the coefficients (2.13) are called the Raynal-Revai coefficients (RRC).

2.4 Schrödinger Equation

The Schrödinger equation for a system of three particles in Jacobi coordinates is written as

$$\left(-\frac{\hbar^2}{2\mu}\left(\nabla^2_{x_i}+\nabla^2_{y_i}\right)+V_{jk}\left(\vec{x}_i,\vec{y}_i\right)+V_{ki}\left(\vec{x}_i,\vec{y}_i\right)+V_{ij}\left(\vec{x}_i,\vec{y}_i\right)-E\right)\Psi\left(\vec{x}_i,\vec{y}_i\right)=0 \tag{2.15}$$

where $\mu=\sqrt{\frac{m_i m_j m_k}{M}}$ is the effective mass parameter.
Substituting equations (2.4) and (2.5) into equation (2.15), the Schrödinger equation is then transformed into hyperspherical coordinates (ρ,Ω_i) as

$$\left(-\frac{\hbar^2}{2\mu}\left\{\frac{1}{\rho^5}\frac{\partial}{\partial\rho}\left(\rho^5\frac{\partial}{\partial\rho}\right)-\frac{\hat{\mathcal{K}}^2\left(\Omega_i\right)}{\rho^2}\right\}+V\left(\rho,\Omega_i\right)-E\right)\ \psi\left(\vec{x}_i,\vec{y}_i\right)\ =\ 0 \tag{2.16}$$

The wavefunction $\Psi\left(\rho,\Omega_i\right)$ expanded in complete sets of the hyperspherical harmonics is defined as the hyperspherical harmonic expansion method and specified as

$$\Psi\left(\rho,\Omega_i\right)=\sum_{k\alpha_i}\frac{U_{k\alpha_i}\left(\rho\right)}{\rho^{\frac{5}{2}}}\mathcal{Y}_{k\alpha_i}\left(\Omega_i\right) \tag{2.17}$$

Substitution of Eq. (2.17) into Eq. (2.6), the use of Eq. (2.8) and considering the orthonormality of hyperspherical harmonics leads to a set of coupled single-variable differential equations

$$\left(-\frac{\hbar^2}{2\mu}\left(\frac{d^2}{d\rho^2}\right)-\frac{\mathcal{L}_K\left(\mathcal{L}_K+1\right)}{\rho^2}-E\right)U_{k\alpha_i}\left(\rho\right)+\sum_{K'\alpha'_i}\left\langle K\alpha_i\right|V\left(\rho,\Omega_i\right)\left|K'\alpha'_i\right\rangle U_{K'\alpha'_i}\left(\rho\right)=0 \tag{2.18}$$

depending only on ρ, where $\mathcal{L}_K=K+\frac{3}{2}$ and

$$\left\langle K\alpha_i\right|V\left|K'\alpha'_i\right\rangle=\int\mathcal{Y}^*_{K\alpha_i}(\Omega_i)V\left(\rho,\Omega_i\right)\mathcal{Y}_{K'\alpha'_i}\left(\Omega_i\right)d\Omega_i \tag{2.19}$$

For the central potential, a large portion of the five-dimensional integrals must be done numerically that makes calculations difficult and imprecise. Be that as it may, the calculation of the matrix (2.11) can be enormously simplified utilizing the unitary transformation (2.12).

2.5 Faddeev Equations

The total wavefuntion for a system of three particles in the Faddeev approach is defined by three amplitudes $\Psi(\vec{x}_i,\vec{y}_i)$. The total three-body wavefunction in Jacobi coordinates is given by $\Psi=\Psi_1\left(\vec{x}_1,\vec{y}_1\right)+\Psi_2\left(\vec{x}_2,\vec{y}_2\right)+\Psi_3\left(\vec{x}_3,\vec{y}_3\right)$. The Faddeev coupled equations are defined by

[26]

$$\begin{aligned}(T_1 + V_1 - E)\,\Psi_1 &= -V_1\,(\Psi_2 + \Psi_3)\\ (T_2 + V_2 - E)\,\Psi_2 &= -V_1\,(\Psi_3 + \Psi_1)\\ (T_3 + V_3 - E)\,\Psi_3 &= -V_3\,(\Psi_1 + \Psi_2)\end{aligned} \tag{2.20}$$

where T_i are the relative kinetic energy operators of each Jacobi partition and V_i the two body interactions potential.

The Faddeev equation in Jacobi coordinates is defined as

$$\Psi_i\,(x_i, y_i) = \sum_{s_c} \psi_{s_c}\,(x_i, y_i) \tag{2.21}$$

where $i = 1, 2, 3$ and ψ_{s_c} comprises of the spin, radial and angular of the two particles relative to the core. Substituting the hyperspherical harmonic expansion, (2.17) and using the hyperspherical coordinates, (2.4) and (2.5), in the Faddeev Equations, gives to a set of coupled equations

$$\left(-\frac{\hbar^2}{2m}\frac{d^2}{d\rho^2} + \hbar^2\frac{\left(K_i + \frac{3}{2}\right)\left(K_i + \frac{5}{2}\right)}{2m\rho^2} - E\right) X^i_{\alpha_i K_i}\,(\rho) + \sum_{j\alpha_j K_j} V^{ij}_{\alpha_i K_i, \alpha_j K_j}\,(\rho)\, X^j_{\alpha_j K_j}\,(\rho) = 0 \tag{2.22}$$

where $V^{ij}_{\alpha_i K_i, \alpha_j K_j}\,(\rho) = \langle \varphi^{l_{x_j} l_{y_j}}_{K_j}\,(\theta_j)\,|\hat{V}_{ij}|\varphi^{l_{x_i} l_{y_i}}_{K_i}\,(\theta_i)\rangle$ is the hyperangular of the two-body interactions.

Chapter 3

Results and Discussion

The computer code FaCE [26] was used, this is a tool that uses the three-body Faddeev equations to calculate the ground state energy, rms radius and wavefunction for halo nuclei three-body nuclei ^{8}B, ^{6}He, ^{6}Li, ^{6}Be, ^{9}Be, ^{9}B treated as three-body systems. These measurements are compared with experimental and theoretical literature.

$$V(\vec{r}) = V_c(r) + \vec{L} \cdot \vec{S}\, V_{so}(r) \tag{3.1}$$

where $V_c(r)$ is the central and $V_{so}(r)$ is the spin-orbit part of the potential. $\vec{L}$ is the orbital angularmomentum and $\vec{S}$ is the spin angularmomentum.

In some cases, the model the central part of the potential with the Wood-Saxon (ws) terms given by equation 3.2 [26]

$$V^i_{ws}(r) = \sum_{k=1,4} p_a(k,i) \left[1 + exp\left(\frac{r - p_a(k+1,i)}{p_a(k+2,i)}\right)\right]^{-1} \tag{3.2}$$

The also model the spin-orbit part of the potential with the Wood-Saxon terms given by equation 3.3

$$V^i_{ws}(r) = \sum_{k=1,4} \frac{p_{so}(k,i)}{r\, p_{so}(k+2,i)} \frac{exp\left(\frac{r-p_{so}(k+1,i)}{p_{so}(k+2,i)}\right)}{\left[1 + \exp\left(\frac{r-p_{so}(k+1,i)}{p_{so}(k+2,i)}\right)\right]^2} \tag{3.3}$$

In other cases, the model with the central and spin-orbit part of the potential with the Gaussian (gau) terms given by equation 3.4

$$V^{i}_{gau}(r) = \sum_{k=1,3,5} p_a(k,i) exp\left[-\left(\frac{r}{p_a(k+1,i)}\right)^2\right] \tag{3.4}$$

In equations 3.2, 3.3 and 3.4 p_a and p_{so} are fitting parameters. For a given system, these parameters are adjusted using experimental data.

3.1 ^{8}B $\rightarrow \alpha +$ ^{3}He + p

The three-body ^{8}B $\rightarrow$ $\alpha +$ ^{3}He + p system is of special importance due to its relevance in the study of nucleosynthesis and the solar boron neutrino problem [5]. The three-body ^{8}B system is considered to have a proton halo and to be the first proton drip line nucleus. Below are the potential input parameters for each interacting pair of the ^{8}B $\rightarrow$ $\alpha +$ ^{3}He + p system.

Table 3.1: Potentials input parameters for interacting pair ^{4}He + ^{3}He.

Coulomb potential [26]:	3.09			
Central potential type:	*gau*			
s-wave	400	1.75	-122.2	2.1
p-wave	300	1.43	-141.6	2.1
f-wave	-48.5	3.1		
Spin-orbit potential type:	*gau*			
p-wave	-2.3	2.1		
f-wave	-13.2	1.91		

Table 3.2: Potentials input parameters for interacting pair ^{4}He + p.

Coulomb potential [26]:	1.46		
Central potential type:	*ws*		
s-wave	43	2	0.7
p-wave	-43	2	0.7
d-wave	-7	2	0.7
Spin-orbit potential type:	*ws*		
p-wave	-40	1.5	0.35
d-wave	-40	1.5	0.35

Table 3.3: Potentials input parameters for interacting pair ^{3}He + p.

Coulomb potential [26]:	1.46					
Central potential type:	ws					
s-wave	350	1.43	0.7	-33	2	0.7
p-wave	-35	2	0.7			
d-wave	350	1.43	0.7	-33	2	0.7
f-wave	-35	2	0.7			
Spin-orbit potential type:	ws					
all-waves	-19.6	1.5	0.35			
Spin-spin potential type:	ws					
s-wave	200	1.43	0.7			
p-wave	-2.7	2	0.7			
d-wave	200	1.43	0.7			
f-wave	-2.7	2	0.7			

The calculated the ground state energy of the system by increasing maximum hyperangularmomentum from $K_{max} = 0$ to $K_{max} = 40$. The mass, charge and radius for each of the three interacting nuclei were adjusted and the total spin and parity were also adjusted for each system. The convergence of the calculated 2^+ ground state energy of the ^{8}B nucleus is shown in figure 3.1. It can be seen that in figure 3.1, the calculated energy converges to 1.798 MeV. The ground state energy obtained is close to the experimental value 1.725 MeV reported in [28], with a variance of 4.06%. As shown in Table 3.4 the results in the literature [5, 29, 30] are consistent.

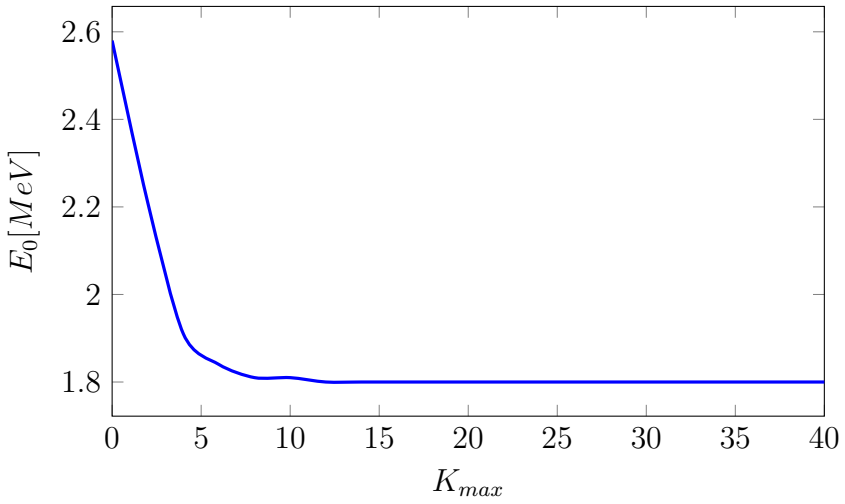

Figure 3.1: Variation of the ground state energy for ^{8}B with increasing total hyperangularmomentum.

Table 3.4: Values of the ground state energy (MeV) for ^{8}B from experimental and theoretical studies.

Experiment		Theoretical	
1.725	[28]	1.874	[5]
		1.665	[29]
		1.78	[30]
		1.798	**This work**

The calculated the root mean square (rms) radius of the system by increasing the maximum hyperangularmomentum from $K_{max} = 0$ to $K_{max} = 40$. The mass, charge and radius for each of the three interacting nuclei were adjusted and the total spin and parity were also adjusted for each system. The convergence of the calculated 2^+ ground state rms radius of the ^{8}B nucleus is shown in figure 3.2. It can be seen that in figure 3.2, the calculated rms radius converges to 2.397 fm. This result has a 1.36% variance from the experimental work [28] and is in good agreement with previous studies [29, 31]. The rms radius of the valence proton is 1.75 times larger than the ^{7}Be core, which further validates the speculation of a proton halo in ^{8}B [5].

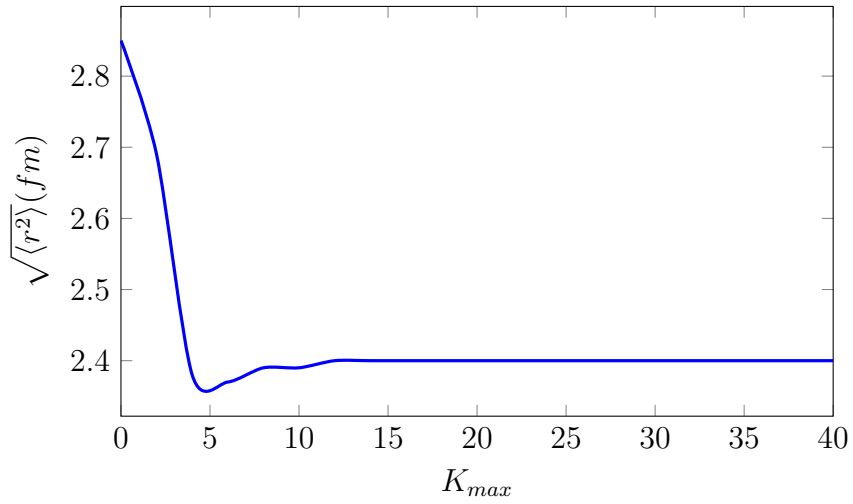

Figure 3.2: Variation of the ground state rms radius for ^{8}B with increasing total hyperangularmomentum.

Table 3.5: Values of the ground state rms radius (fm) for ^{8}B from experimental and theoretical studies.

Experiment		Theoretical	
2.43	[28]	2.38-2.39	[5]
2.45	[29]	**2.397**	**This work**
2.38	[31]		

The wavefunction for the partial waves of the system were also determined. Figure 3.3 is the wavefunctions for the partial waves $K = 0, 2, 4$. It is observed in the figure that the wavefunction for the partial wave $K = 0$ contributes the most to the total wavefunction of the system.

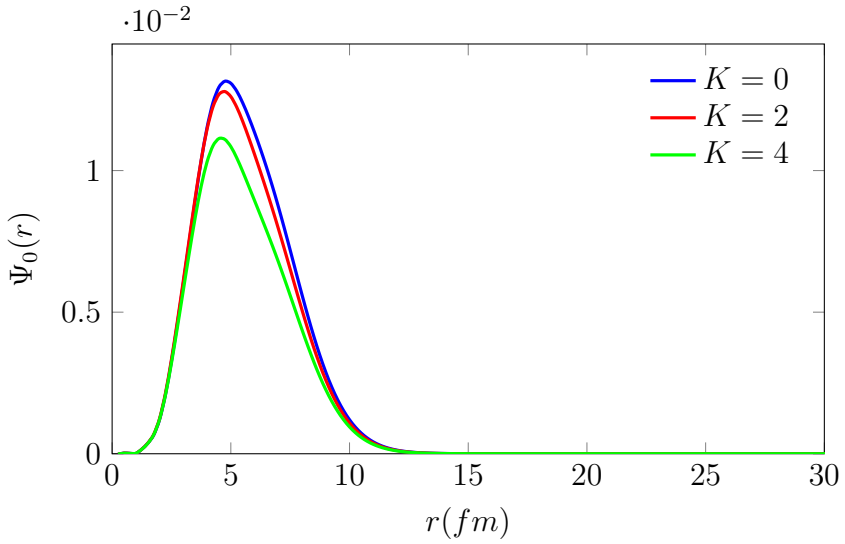

Figure 3.3: Wavefunctions of the ground state for ^{8}B for hyperangularmomentum $K_{max} = 0, 2, 4$.

3.2 ^{6}He $\rightarrow \alpha$ + n + n

The three-body ^{6}He $\rightarrow \alpha$ + n + n system is a Borromean nucleus that, together with ^{11}Li, exhibits a halo structure with two loosely bound valence neutrons [32]. ^{6}He is often used as a benchmark system for three-body exotic loosely bound nuclei since the α - n interaction is better understood. Below are the potential input parameters for each interacting pair for the ^{6}He $\rightarrow \alpha$ + n + n system.

Table 3.6: Potentials input parameters for interacting pair ^{4}He + n.

Central potential type [26]:	*gau*	
s-wave	50	2.35
p-wave	-47.32	2.35
d-wave	-23	2.35
Spin-orbit potential type:	*gau*	
p-wave	-11.71	2.35
d-wave	-11.71	2.35

Table 3.7: Potentials input parameters for interacting pair n + n.

Central potential type [26]:	ws	
s-wave	-31	1.8

The calculated the ground state energy similarly to that in the previous section. The convergence of the calculated 0^+ ground state energy of the ^{6}He nucleus is shown in figure 3.4. It can be seen that in figure 3.4, the calculated energy converges to 0.862 MeV. The ground state energy obtained is close to the experimental value 0.975 MeV reported in [33], with a variance of 11.59%. As shown in table 3.8, the results are consistent with literature [34, 35, 36].

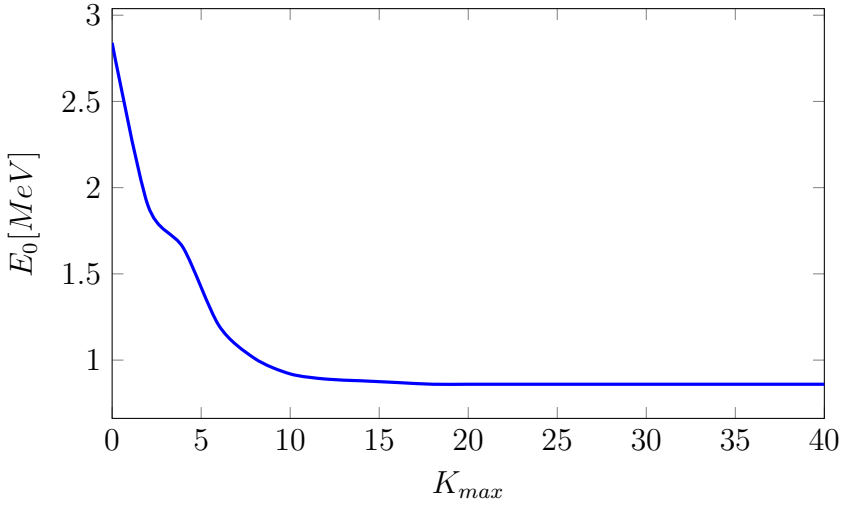

Figure 3.4: Variation of the ground state energy for ^{6}He with increasing total hyperangularmomentum.

Table 3.8: Values of the ground state energy (MeV) for ^{6}He from experimental and theoretical studies.

Experiment		Theoretical	
0.975	[33]	0.98	[36]
0.976	[34]	**0.862**	**This work**
0.973	[35]		

The ground state rms radius was calculated as stated in the previous section. The convergence of the calculated 0^+ ground state rms radius of the ^{6}He nucleus is shown in figure

3.5. It can be seen that in figure 3.5, the calculated rms radius converges to 2.557 fm. The ground state rms radius obtained is close to the experimental value 2.57 fm reported in [37], with a variance of 0.51%. As shown in table 3.9, the results are consistent with literature [36, 39, 40].

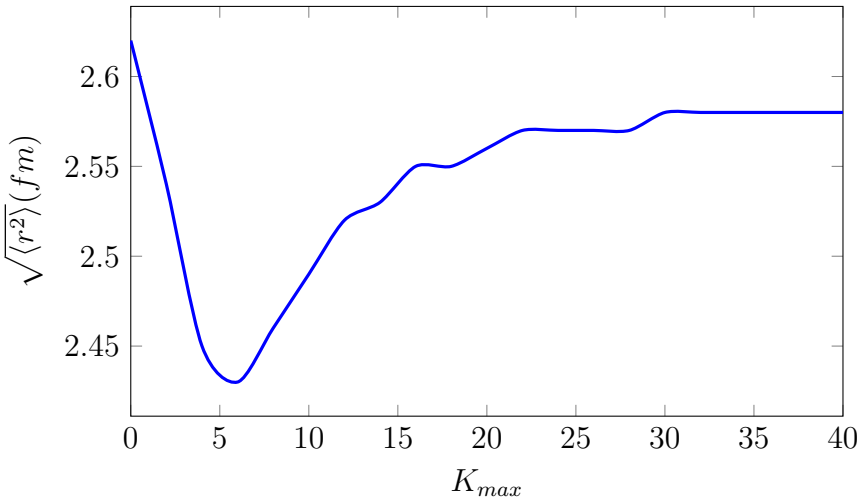

Figure 3.5: Variation of the ground state rms radius for ^{6}He with increasing total hyperangularmomentum.

Table 3.9: Values of the ground state radius (fm) for ^{6}He from experimental and theoretical studies.

Experiment		Theoretical	
2.57	[37]	2.51	[36]
2.48	[38]	2.51	[39]
		2.5	[40]
		2.557	**This work**

Figure 3.6, is the wavefunctions for the partial waves $K = 0, 2, 4$. It is observed in the figure that the wavefunction for the partial wave $K = 0$ contributes the most to the total wavefunction of the system.

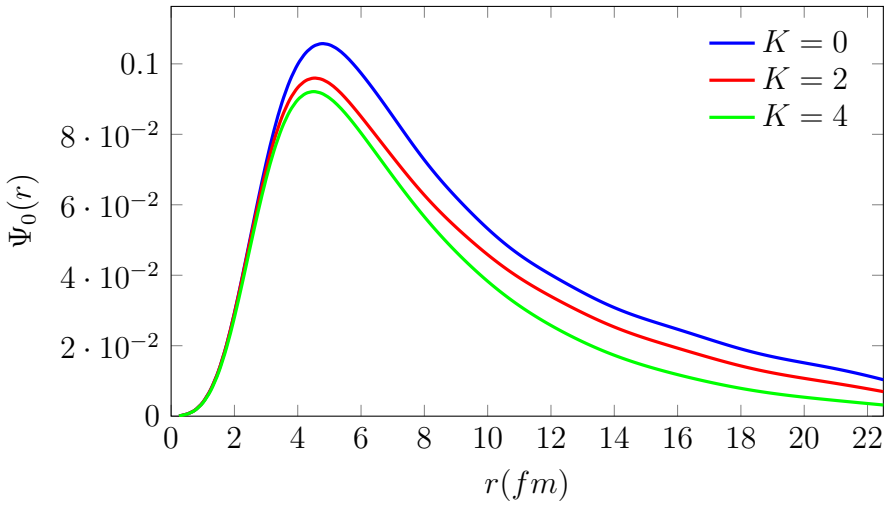

Figure 3.6: Wavefunction of the ground state for ^{6}He for hyperangularmomentum $K_{max} = 0, 2, 4$.

3.3 ^{6}Li $\rightarrow \alpha$ + n + p

The application of the three-body ^{6}Li $\rightarrow$ α + n + p system is of interest since deuteron induced reactions are generally used to examine astrophysical data and nuclear structure [8]. The potential input parameters for the interacting pair ^{4}He + n is shown in table 3.6 and the potential input parameters for ^{4}He + p is shown in table 3.2. The potential input parameters for n + p is shown in table 3.10 below.

Table 3.10: Potentials input parameters for interacting pair n + p.

Central potential type [26]:	ws	
s-wave	-31	1.8

The calculation of the ground state energy was performed as mentioned above. The convergence of the calculated 1^+ ground state energy of the ^{6}Li nucleus is shown in figure 3.7. It can be seen that in figure 3.7, the calculated energy converges to 3.307 MeV. The ground state energy obtained is close to the experimental value 3.6989 MeV reported in [35], with a variance of 10.60%. As shown in table 3.11, the results are consistent with literature [41, 42, 43].

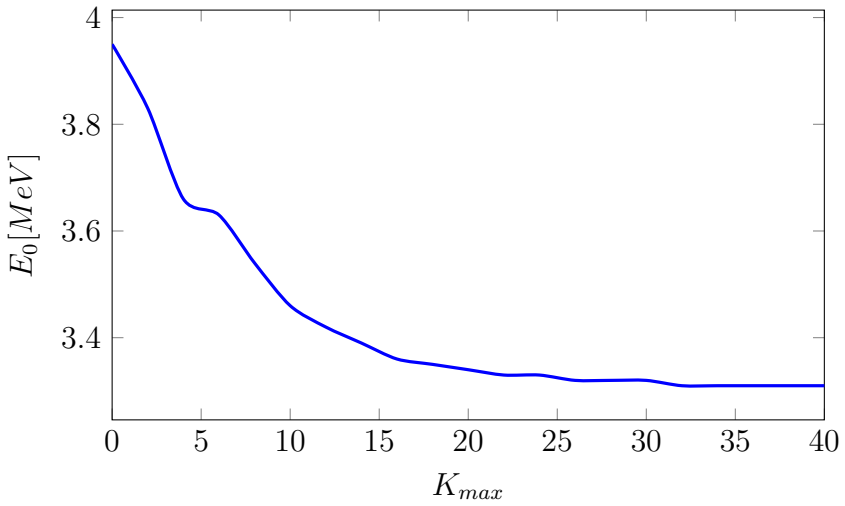

Figure 3.7: Variation of the ground state energy for ^{6}Li with increasing total hyperangularmomentum.

Table 3.11: Values of the ground state energy (MeV) for ^{6}Li from experimental and theoretical studies.

Experiment		Theoretical	
3.6989	[35]	3.6	[41]
		3.7	[42, 43]
		3.307	**This work**

The ground state rms radius is calculated similarly to that in the previous section. The convergence of the calculated 1^+ ground state rms radius of the ^{6}Li nucleus is shown in figure 3.8. It can be seen that in figure 3.8, the calculated rms radius converges to 2.694 fm. The ground state rms radius obtained is close to the experimental value 2.54 fm reported in [42], with a variance of 5.49%. As shown in table 3.12, the results are consistent with literature [43, 44].

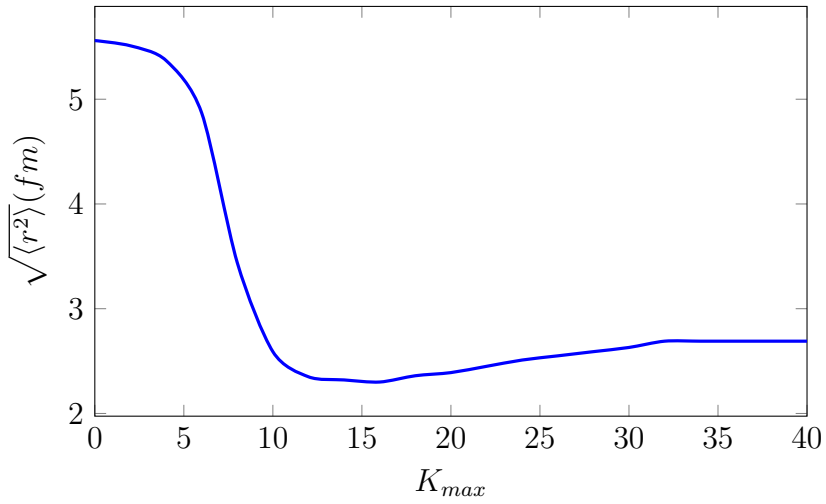

Figure 3.8: Variation of the ground state rms radius for ^{6}Li with increasing total hyperangularmomentum.

Table 3.12: Values of the ground state radius (fm) for ^{6}Li from experimental and theoretical studies.

Experiment		Theoretical	
2.54	[42]	2.51	[44]
2.5	[43]	**2.694**	**This work**

Figure 3.9 is the wavefunctions for the partial waves $K = 0, 2, 4$. It is observed in the figure that the wavefunction for the partial wave $K = 0$ contributes the most to the total wavefunction of the system.

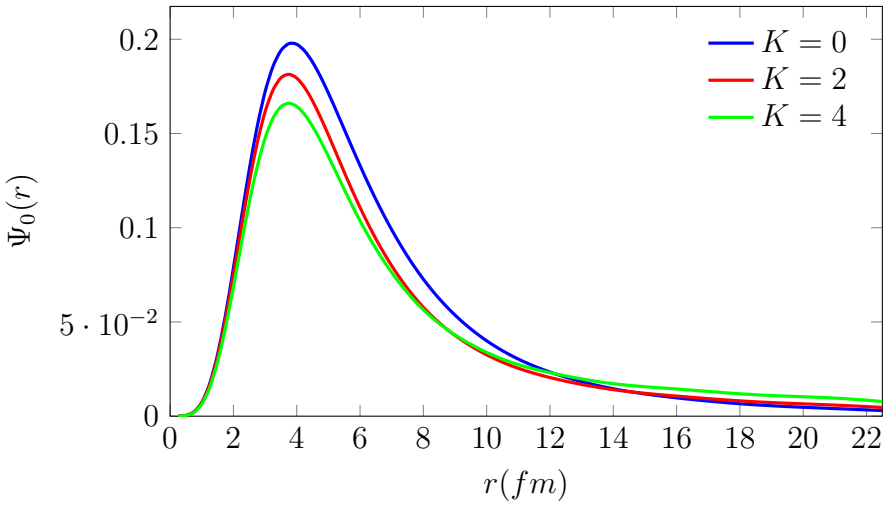

Figure 3.9: Wavefunction of the ground state for ^{6}Li for hyperangularmomentum $K_{max} = 0, 2, 4$.

3.4 ^{6}Be $\rightarrow \alpha$ + p + p

The three-body ^{6}Be $\rightarrow \alpha$ + p + p is of special interest due to the fact that ^{6}Be is the lightest two-proton emitter and is crucial in the study of two proton decay [45]. The potential input parameters for the interacting pair ^{4}He + p is shown in table 3.2.

The ground state energy was calculated as stated in the previous section. The convergence of the calculated 0^+ ground state energy of the ^{6}Be nucleus is shown in figure 3.10. It can be seen that in figure 3.10, the calculated energy converges to 1.277 MeV. The ground state energy obtained is close to the experimental value 1.371 MeV reported in [35], with a variance of 8.79%. As shown in table 3.13, the results are consistent with literature [46, 47].

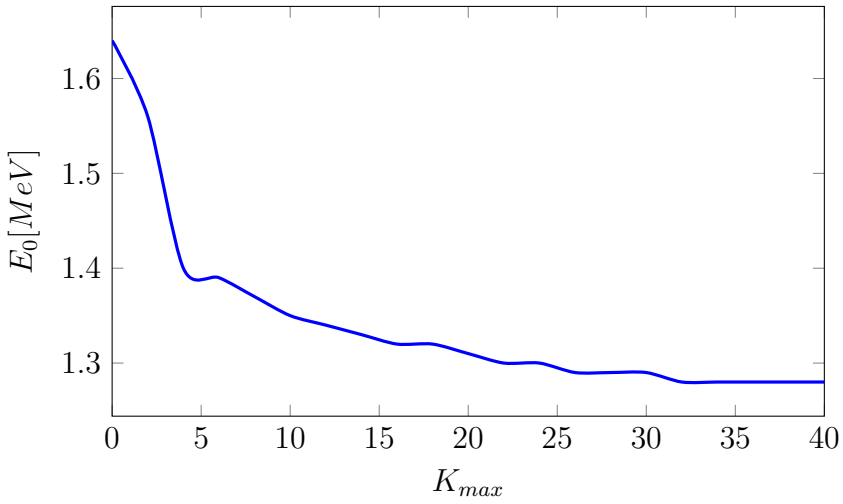

Figure 3.10: Variation of the ground state energy for ^{6}Be with increasing total hyperangularmomentum.

Table 3.13: Values of the ground state energy (MeV) for ^{6}Be from experimental and theoretical studies.

Experiment		Theoretical	
1.371	[35]	3.7	[47]
1.37	[46]	**1.277**	**This work**

The calculation of the ground state rms radius was done as mentioned above. The convergence of the calculated 0^+ ground state rms radius of the ^{6}Be nucleus is shown in figure 3.11. It can be seen that in figure 3.11, the calculated rms radius converges to 2.872 fm. The ground state rms radius obtained is close to the experimental value 2.96 fm reported in [48], with a variance of 5.49% as shown in table 3.14.

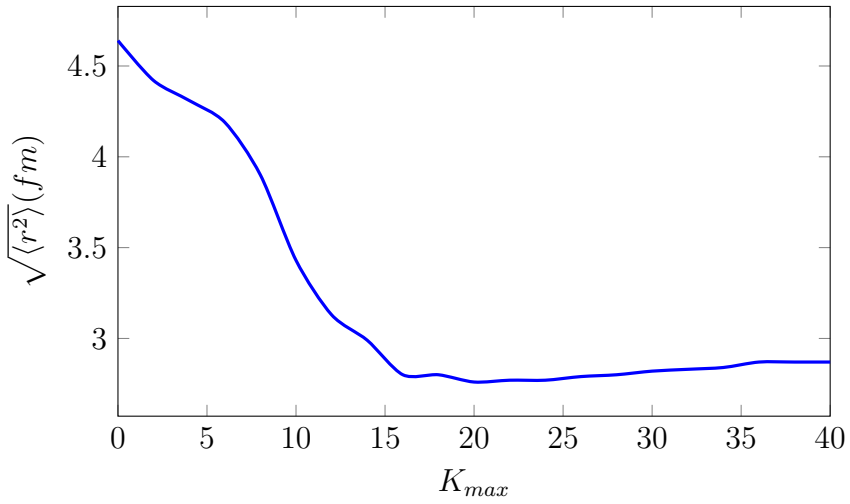

Figure 3.11: Variation of the ground state rms radius for ^{6}Be with increasing total hyperangularmomentum.

Table 3.14: Values of the ground state radius (fm) for ^{6}Be from experimental and theoretical studies.

Experiment	Theoretical
2.96 [48]	**2.872 This work**

Figure 3.12 is the wavefunctions for the partial waves $K = 0, 2, 4$. It is observed in the figure that the wavefunction for the partial wave $K = 0$ contributes the most to the total wavefunction of the system.

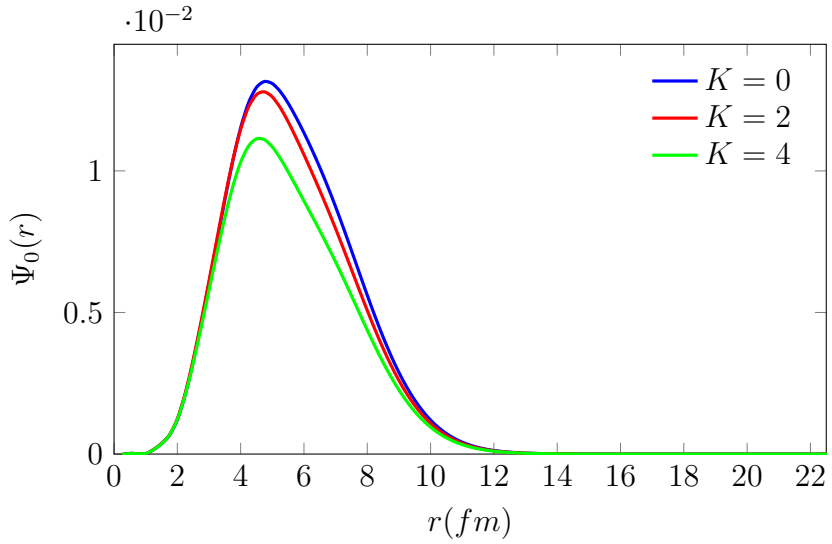

Figure 3.12: Wavefunction of the ground state for ^{6}Be for hyperangularmomentum $K_{max} = 0, 2, 4$.

3.5 ^{9}Be $\rightarrow \alpha + \alpha +$ n

The three-body ^{9}Be $\rightarrow \alpha + \alpha +$ n is considered to be the only bound ground state and all excited states lie above the three-body threshold [7]. Hence ^{9}Be is expected to have low-lying state. Below are the potential input parameters for each interacting pair of the ^{9}Be $\rightarrow \alpha + \alpha$ + n system.

Table 3.15: Potentials input parameters for interacting pair ^{4}He + ^{4}He.

Coulomb potential	1.35
Central potential type [49]:	ws
s-wave	175
p-wave	-0.63
d-wave	0.001
f-wave	30
g-wave	-0.24

Table 3.16: Potentials input parameters for interacting pair n + n.

Central potential type [26]:	ws	
s-wave	-31	1.8

The calculated the ground state energy similarly to that in the previous section. The convergence of the calculated $\frac{3}{2}^-$ ground state energy of the ^{9}Be nucleus is shown in figure 3.13. It can be seen that in figure 3.13, the calculated energy converges to 1.443 MeV. The ground state energy obtained is close to the experimental value 1.371 MeV reported in [35], with a variance of 8.10%. As shown in table 3.17, the results are consistent with literature [50, 51, 52].

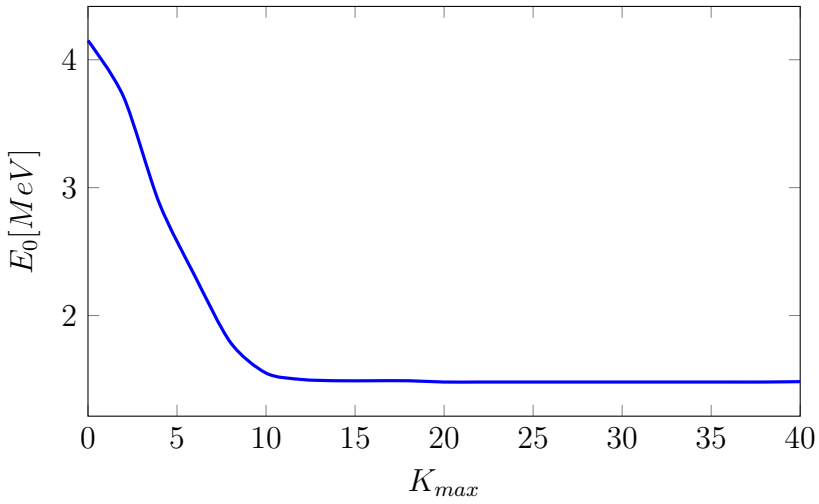

Figure 3.13: Variation of the ground state energy for ^{9}Be with increasing total hyperangularmomentum.

Table 3.17: Values of the ground state energy (MeV) for ^{9}Be from experimental and theoretical studies.

Experiment		Theoretical	
1.5736	[35]	1.572	[52]
1.57	[50, 51]	**1.443**	**This work**

The ground state rms radius was calculated as stated in the previous section. The convergence of the calculated $\frac{3}{2}^-$ ground state rms radius of the ^{9}Be nucleus is shown in figure 3.14. It can be seen that in figure 3.14, the calculated rms radius converges to 2.71 fm. The ground state rms radius obtained is close to the experimental value 2.518 fm reported in [46], with a variance of 4.63%. As shown in table 3.18, the results are consistent with literature [47, 48].

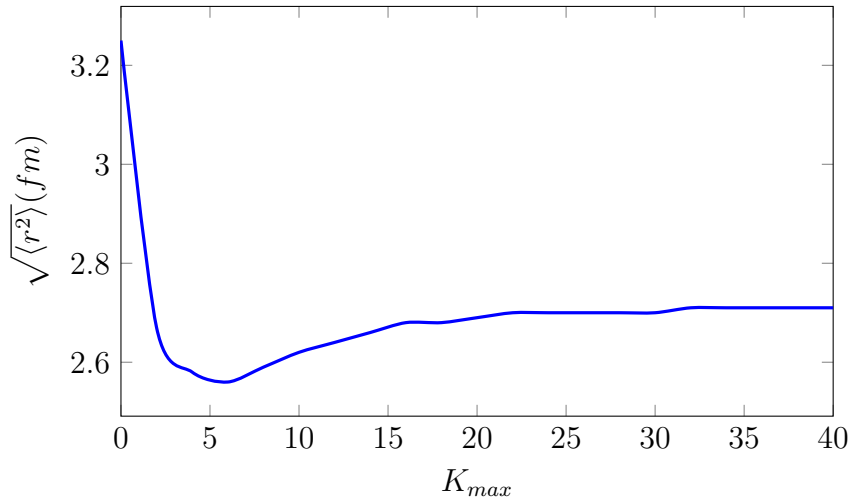

Figure 3.14: Variation of the ground state rms radius for ^{9}Be with increasing total hyperangularmomentum.

Table 3.18: Values of the ground state radius (fm) for ^{9}Be from experimental and theoretical studies.

Experiment		Theoretical	
2.518	[46]	2.59	[48]
2.59	[47]	**2.71**	**This work**

Figure 3.15 is the wavefunctions for the partial waves $K = 0, 2, 4$. It is observed in the figure that the wavefunction for the partial wave $K = 0$ contributes the most to the total wavefunction of the system.

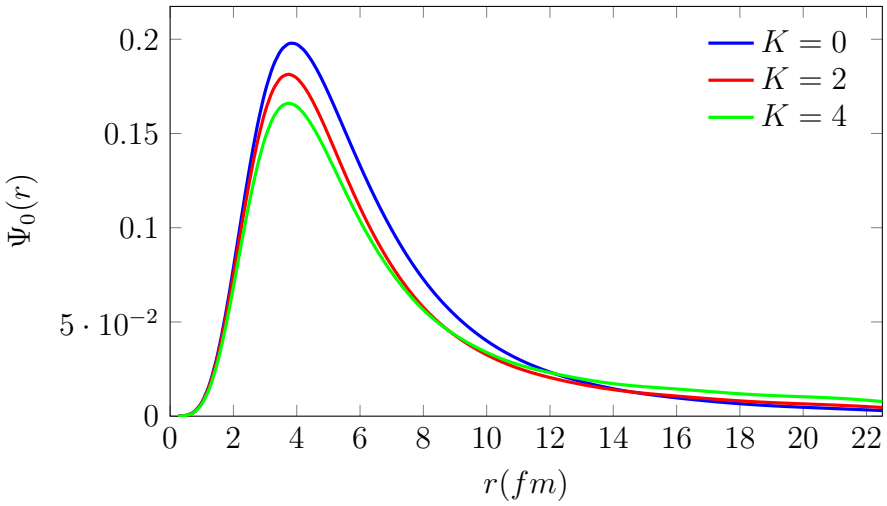

Figure 3.15: Wavefunction of the ground state for ^{9}Be for hyperangularmomentum $K_{max} = 0, 2, 4$.

3.6 $^9\mathbf{B} \rightarrow \alpha + \alpha + \mathbf{p}$

Like mirror nucleus ^{9}Be, the three-body ^{9}B $\rightarrow \alpha + \alpha +$ p system has low-lying levels and considered to be a Borromean system [7]. The potential input parameters for interacting pairs ^{4}He + ^{4}He and ^{4}He + p are shown in table 3.15 and table 3.2 respectively.

The calculation the ground state energy was done as mentioned above. The convergence of the calculated $\frac{3}{2}^-$ ground state energy of the ^{9}B nucleus is shown in figure 3.16. It can be seen that in figure 3.16, the calculated energy converges to 0.202 MeV. The ground state energy obtained is in close proximity to the experimental value 0.28 MeV reported in [50], with a variance of 27.9%. As shown in table 3.19, the results are consistent with literature [53, 54].

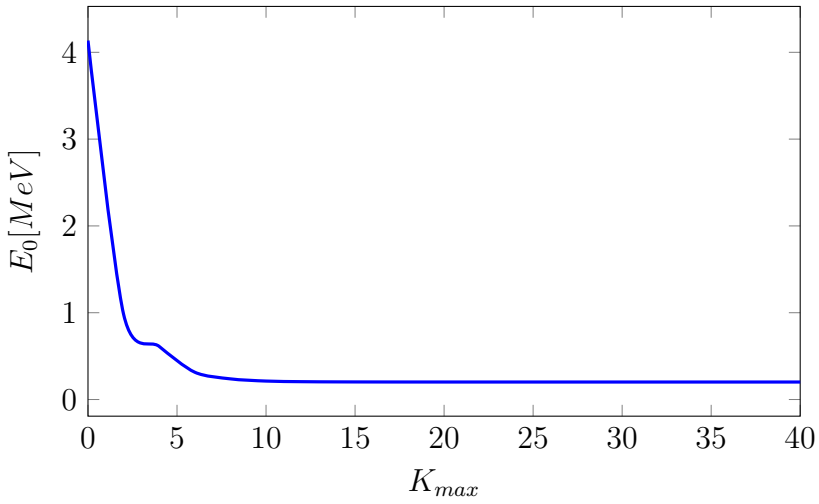

Figure 3.16: Variation of the ground state energy for ^{9}B with increasing total hyperangularmomentum.

Table 3.19: Values of the ground state energy (MeV) for ^{9}B from experimental and theoretical studies.

Theoretical	
0.28	[50]
0.277	[53, 54]
0.202	**This work**

The calculated the ground state rms radius similarly to that in the previous section. The convergence of the calculated $\frac{3}{2}^-$ ground state rms radius of the ^{9}B nucleus is shown in figure 3.17. It can be seen that in figure 3.17, the calculated rms radius converges to 2.92 fm. The ground state rms radius obtained is close to the experimental value 2.81 fm reported in [55], with a variance of 3.56% as shown in table 3.20.

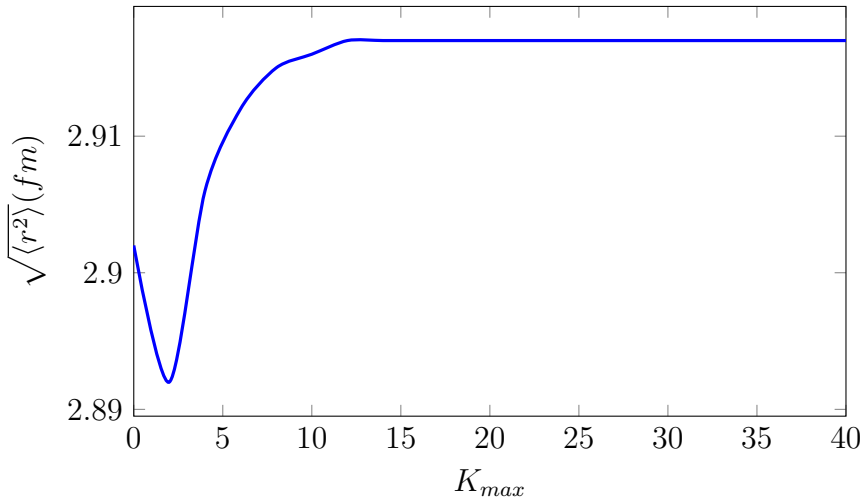

Figure 3.17: Variation of the ground state rms radius for ^{9}B with increasing total hyperangularmomentum.

Table 3.20: Values of the ground state radius (fm) for ^{9}B from experimental and theoretical studies.

Theoretical	
2.81	[55]
2.92	**This work**

Figure 3.18 is the wavefunctions for the partial waves $K = 0, 2, 4$. It is observed in the figure that the wavefunction for the partial wave $K = 0$ contributes the most to the total wavefunction of the system.

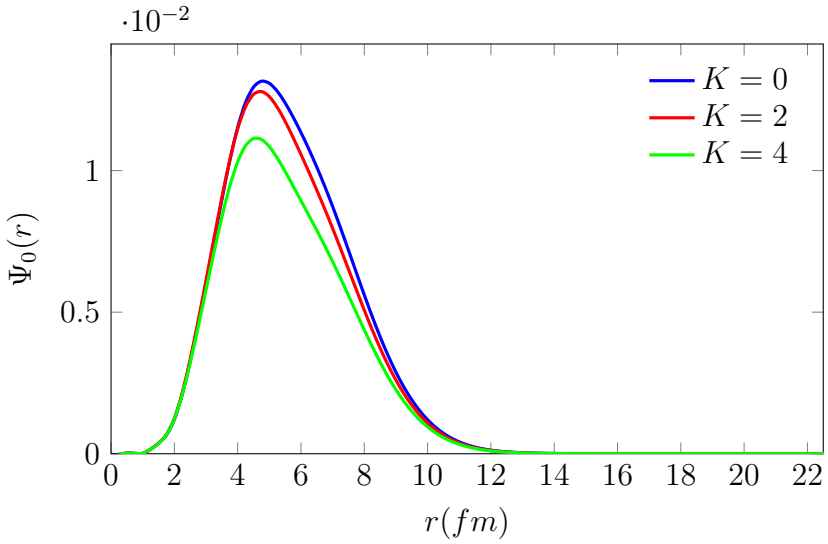

Figure 3.18: Wavefunction of the ground state for ^{9}B for hyperangularmomentum $K_{max} = 0, 2, 4$.

Chapter 4

Concluding Remarks

The aim for this research is to investigate the nuclear structural properties of three-body nuclei systems in particular the halo nuclei. The three-body systems ^{8}B, ^{6}He, ^{6}Li, ^{6}Be, ^{9}Be and ^{9}B were identified to investigate the properties of a halo nuclei system and confirm if these systems are indeed halo nuclei. In order to achieve this, the calculated ground state energy, ground state root-mean-square radii and determined the wavefunctions for partial waves $K = 0, 2, 4$ for each system. From these results, investigation on whether these systems are indeed halo nuclei were performed. Further investigation the on different properties between a proton and neutron halo nuclei were performed. Investigation on the different properties between a two-neutron and a single-neutron halo system were also performed. The results were compared with theoretical and experimental literature, the accuracy and variances were recorded. To achieve these results, the trusted program called FaCE was used. The purpose of this program is to attain bound state structural configurations for light exotic nuclei three-body systems. The program was used to study the systems because halo nuclei have a low binding energy, the systems are light nuclei and are three-body systems. The input files were adjusted for each system as follows: the potential input parameters for each two-body interacting pair were adjusted for each system. The mass, charge and radius for each of the three interacting nuclei were adjusted and the total spin and parity were also adjusted for each system.

The ground state energy was calculated by increasing the maximum angularmomentum from $K_{max} = 0$ to $K_{max} = 40$. Convergence of the ground state energy was observed, and the convergence energy was compared to experimental and theoretical literature. The variance was noted and recorded. For the ground state root-mean-square, a similar process was

followed, the convergence root-mean-square was obtained by increasing the maximum angularmomentum $K_{max} = 0$ to $K_{max} = 40$ The convergent root-mean-square was then compared with literature and the variance were captured. The wavefunction for the partial waves $K = 0, 2, 4$ was also determined and the wavefunction for the partial wave that contributed the most to the wavefunction was observed.

The results obtained were in good agreement with previous theoretical and experimental work. It was found that the results obtained were slightly overestimated. The ground state root-mean-square radius results were found to be more accurate than the ground-state energy results. As stated by the creators of the FaCE program [26] , discrepancies in the results could be because the program uses a predetermined Feshbach energy instead of recalculating for each eigen energy and the diagonalization method used is efficient for the initial energy E_0 being lower than the ground state energy, where there are no close degenerate eigenvalues nearby.

The neutron halo three-body systems that were chosen to investigate where ^{6}He, ^{6}Li and ^{9}Be. The evidence that these systems were indeed neutron halo systems could indicate the wavefunctions which exhibit a long tail which indicates that their density probability lies outside the range of the core potential. The systems convergent root-mean-square radius are large in size. The systems ^{6}He and ^{9}Be show low ground state energies whereas ^{6}Li has a significantly higher ground state energy than ^{6}He and ^{9}Be, since ^{6}Li does not appear close to the neutron dripline, but it does have a long tail like wavefunction and a relatively large root-mean-square radius which would indicate that ^{6}Li could be a neutron halo. The wavefunctions for the partial waves $K = 0$ were most dominant and contributed the most to the total wavefunction which further indicates that these systems are halo nuclei systems, since halo nuclei have a very low angularmomentum. ^{6}He is a special halo nuclei since it exhibits two loosely bound valence neutrons. A comparison of ^{6}He with the single-neutron halo systems ^{6}Li and ^{9}Be show that the two-neutron halo has a lower ground state energy than single-neutron halo system. The ground state root-mean-square radius of the two-neutron halo system ^{6}He is similar to the single-neutron halo system ^{6}Li, which would indicate that the size of a single-neutron halo is similar to that of a two-neutron halo nuclei.

The Coulomb and centrifugal barrier for proton halo nuclei means that the valence proton is located closer to the core than the neutron halo nuclei. This makes proton halo nuclei rarer

and more difficult to identify. The systems chosen to investigate proton halo three-body systems are ^{8}B, ^{6}Be and ^{9}B. The main evidence that these systems are proton halo nuclei is given by the distribution of the wavefunction which have a long tail (not as predominant as neutron halo nuclei). The systems wavefunction for the partial waves is dominant at $K = 0$. The systems also have a relatively a low ground state energy and large ground state root-mean-square radius which further validates that these systems are proton halo nuclei systems. To compare the properties of neutron and proton halo nuclear systems, a comparison between the ^{8}B (proton halo) and the ^{9}Be (neutron halo) was performed. Since both systems are well considered halo nuclei by literature, have a single valence nucleon and have a similar core structure. It can be seen from the results that ^{8}B has a smaller root-mean-square radius, larger ground state energy and shorter tail wavefuntion than ^{9}Be. This would further indicate the existence of the Coulomb barrier keeps the valence proton closer to the core compared to the neutron halo nuclei. In conclusion, based on the results in this literature, this dissertation can confirm the three-body nuclei systems investigated are halo nuclei. The distinction between a proton halo and neutron halo is confirmed and the distinctions between a two-neutron halo and one-neutron halo has also been confirmed.

Bibliography

[1] I.Tanihata, Phys. World **12** 22 (1999).

[2] E.K. Warbuton, Revista Brasileira de Física **2** 37-59 (1972).

[3] J.S. Al-Khalili, Lecture Notes in Physics **651** 77-112 (2004).

[4] I. Tanihata, J. Phys. G: Part. Phys. **22** 157-198 (1996).

[5] L. V. Grigorenko et al., Phys. Rev. C. **57** 2099 (1998).

[6] L. V. Grigorenko et al., Phys. Rev. C. **651** 77-112 (2004).

[7] K. Arai et al., Phys. Rev. C. **68** 014310 (2003).

[8] L. Hlophe et al., Phys. Rev. C. **96** 064003 (2017).

[9] R.C.J. Russell (2012), *Faddeev Equations*, Russia, Bookvika Publishing

[10] C.Elster et al., Few-Body Systems **27** 83-105 (1999).

[11] Z. Ma, Founds of Physics Letters **12** 561-570 (1999).

[12] T. K. Das, S.K. Bhattacharyya, J. Phys. **40(3)** 189-200 (1993).

[13] A.C. Phillips, Physical Review **142(4)** 984-989 (1966).

[14] P. Belov, S.L. Yakovlev, Bulletin of the Russion Academy of Sciences Physics **76(8)** 1016-1021 (2012).

[15] D.S. Chuu, C.S. Han, Chinese journal of Physics **13(1)** 60-68 (1975).

[16] C.P. Carpenter, T.F. Tuan, Phys. Rev. A. **2(5)** 1811 (1970).

[17] G.F. Drukarev, S.A. Pozdneev, Sov. Phys. JETP **47** 2009-2016 (1978).

[18] A. Nannini, L.E. Marcucci Front. Phys. **6** 122 (2018).

[19] A. Cobis, D.V. Fedorov, A.S. Jensen, Nucl. Phys. C. **58** 1403-1421 (1998).

[20] S.M. Motevalli, (2012), *Applications of Quantum Mechanics*, InTech, Rijeka, Croatia.

[21] A. Khan et al., FIZIKA B (Zagreb) **8(4)** 469-482 (1999).

[22] R. Krivec, Few-Body Systems **25** 199-238 (1998).

[23] M.A. Allam, Journal of Applied Physics **2(2)** 30-36 (2012).

[24] J.S. Avery, Journal of Computational and Applied Mathematics. **233** 1366–1379 (2010).

[25] S. Rosati, Series on Advances in Quantum Many-Body Theory **7** 339-378 (2002).

[26] I.J. Thompson et al., Computer Physics Communications **161** 87–107 (2004).

[27] S.N. Ershov, (2004), *Halo Nuclei*, Joint Institute for Nuclear Research.

[28] F. Ajzenberg-Selove, Nucl. Phys. A. **490** 1 (1998).

[29] M. Fukuda et al., Nucl. Phys. A. **656** 209 (1999).

[30] K. Varga, Y. Suzuki and I. Tanihata, Phys. Rev. C. **52** 3013 (1995).

[31] L.Tanihata et al., Phys. Lett. B. **206** 592 (1988).

[32] J.S. Vaagen et al., Z. Phys. A. **349** 285 (1994).

[33] V.Lapoux, N. Alamanos, F. Auger, A. Drouart, Nucl. Phys. A. **722** 01334-4 (2002).

[34] A. H. Wapstra, G. Audi, R. Hoekstra, At. Data Nucl. Data Tables **39** 281 (1988).

[35] D.R. Tilley, Nucl. Phys. A. **708**0 3-163 (2002).

[36] I. J. Thompson et al., Phys. Rev. C. **61** 024318 (2000).

[37] I Tanihata et al., Riken, Preprint AF-NP-60 (1978).

[38] L. Chulkov et al., Europhys., Phys. Lett. **8** 245 (1989).

[39] I. J. Thompson et al., Phys. Rev. C. **61** 024318 (2000).

[40] E. Garrido, D. V. Fedorov, A. S. Jenson, Nucl. Phys. A. **617** 153 (1997).

[41] A. Hasegawa, S. Nagata, Progress of Theoretical Phys. **45** 6 (1971).

[42] D.C. Zheng et al., Phys. Rev. C. **48** 1083-1091 (1993).

[43] W.A. Wurtz et al., Phys. Rev. C. **90** 014613 (2014).

[44] I. Angeli, K.P. Marinova, Atomic Data and Nuclear Data Tables **99** 69-95 (2013).

[45] L. V. Grigorenko et al., Phys. Rev. C. **80** 034602 (2009).

[46] A.I. Malakhov et al., Exotic Nuclei 67-74 (2013).

[47] V. Chudoba et al., Exotic Nuclei 315-321 (2017).

[48] S. Pieper, The European Physical Journal A: Hadrons and Nuclei **13** 75-79 (2002).

[49] H. Guo, EPJ Web of Conferences **146** 12011(ND2016) (2017).

[50] A.V. Nesterov et al., Physics of Atomic Nuclei **77** 555-568 (2014).

[51] C. Jollet, A. Meregaglia, Nuclear Instruments and Methods in Physics **949** 162904 (2020).

[52] E. Filandri et al., SciPost Physics Proceedings **3** 34 (2020).

[53] M. Odsuren et al., The European Physical Journal Conf. **146** 12012 (2017).

[54] F.C. Barker, Aust. J. Phys. **40** 307-17 (1987).

[55] Q. Zhao, Phys. Rev. C. **97** 054323 (2018).